Available online at www.sciencedirect.com
SCIENCE DIRECT®
Planetary and Space Science 53 (2005) 283–290
Planetary and Space Science
www.elsevier.com/locate/pss

High resolution observations of continuum radiation

J.D. Menietti[a,*], O. Santolik[b,c], J.S. Pickett[a], D.A. Gurnett[a]

[a]Department of Physics and Astronomy, The University of Iowa, 210 Van Allen Hall, Iowa City, IA 52242-1479, USA
[b]Faculty of Mathematics and Physics, Charles University, Prague, Praha 8, Czech Republic
[c]Institute of Atmospheric Physics, Czech Academy of Sciences, 11720 Prague 1, Czech Republic

Accepted 12 September 2004
Available online 15 December 2004

Abstract

The Polar spacecraft has identified near-source regions of continuum emission in the plasmapause and outer plasmasphere. As in the case of kilometric continuum (KC), near-source regions of continuum emission often display a high resolution fine structure of closely spaced bands of emission. The separation of the bands is much less than the local gyrofrequency. This suggests that the source is associated with density structures and perhaps the result of trapped eigenmodes. These results imply further that continuum emission is the low-frequency manifestation of KC emission.

Keywords: Waves in plasmas; Kilometric continuum; Plasmapause

1. Introduction

Brown (1973) and Gurnett and Shaw (1973) first reported terrestrial nonthermal continuum emission in a broad frequency range extending from ~5 kHz to < 100 kHz. The term continuum implied a diffuse, rather continuous spectrum. Gurnett and Shaw (1973) and Gurnett (1975) proposed a source near the dawnside plasmapause, with a source mechanism associated with intense upper hybrid waves. Kurth et al. (1981) and Kurth (1982) described the details of the narrow-banded escaping component of continuum emission providing clear evidence of its narrow-bandedness associated with intense upper hybrid (UH) resonance emissions occurring, where $f_{UH} = (n+1/2)f_{ce}$ (where f_{ce} is the electron cyclotron frequency). These emissions are also believed to have a low-latitude source in the outer plasmasphere and in the magnetopause (cf. Jones, 1988; Morgan and Gurnett, 1991). The source mechanism of this continuum emission has been proposed to be a mode conversion process occurring near the dayside magnetopause and/or the nightside plasmapause near the equator. Both linear (e.g., Jones, 1976, 1988; Budden, 1980) and nonlinear (cf. Melrose, 1981; Fung and Papadopoulos, 1987; Ronnmark, 1983) classes of mode conversion have been suggested as summarized in Kurth (1992).

Kasaba et al. (1998) have reported a new type of terrestrial continuum emission which they call continuum enhancement, observed by the Geotail satellite. These authors describe the emission as a short-lived enhancement that is generated at the plasmapause from the midnight to dawnside sector. The typical or usual nonthermal continuum radiation that is generated at the dayside plasmapause appears to follow the enhanced continuum. Kasaba et al. show evidence that these emissions are generated by a series of electrons injected at the midnight sector and associated with a substorm. The enhanced continuum has both "fast" and "main" components. The fast component displays a more rapid increase of frequency (50–100 kHz/h) and shorter duration (0.5–1 h) than the main component (10–20 kHz/h;

*Corresponding author. Tel.: +1 319 335 1919; fax: +1 319 335 1753.
E-mail address: jdm@space.physics.uiowa.edu (J.D. Menietti).

0032-0633/$ - see front matter © 2004 Elsevier Ltd. All rights reserved.
doi:10.1016/j.pss.2004.09.054

1–3 h duration). The explanation provided is that the fast component is generated at the midnight plasmapause by lower-energy electrons, while the main component is produced by the higher-energy electrons that have gradient and curvature drifted to the dawnside plasmapause. The rate of increase and later decrease of the frequency of these emissions indicates the classic erosion and refilling of the plasmasphere associated with a terrestrial magnetic substorm. The observations of continuum emission presented in the present study (using the Polar and Cluster spacecraft) may or may not be continuum enhancement. While we have noted the magnetic conditions, the polar-orbiting spacecraft passed quickly through the emission region and no long term monitoring observations were possible. Rather, the subject of the present study is the micro or fine structure of the continuum emission, which we believe provides important clues to the structure of the source region and the nature of the generation mechanism.

Hashimoto et al. (1999) have described kilometric continuum (KC) as emission that lies in the same frequency range as auroral kilometric radiation (AKR) (cf. Gurnett, 1974), but with a different spectral morphology and a unique source region, the low-latitude inner plasmasphere. KC was observed by Geotail to consist of slowly drifting narrowband signals in the frequency range $100\,\mathrm{kHz} < \cap f < 800\,\mathrm{kHz}$. Direction-finding using spin modulation of the emission at 400 kHz indicated the source of the emission is consistent with the low-magnetic-latitude inner plasmasphere. The emission thus has much in common with nonterrestrial continuum emission observed at lower frequencies (typically $<100\,\mathrm{kHz}$). More recently, Green et al. (2002) have shown an association of the KC with plasmaspheric bite-outs of density and suggested that these large-structure depletions may be a source region of the KC.

Menietti et al. (2003) have presented plasma wave data from Polar, Geotail, and Cluster that suggest KC emission has a source in the low-latitude plasmasphere as has been argued by Hashimoto et al. (1999). The Polar spacecraft orbit allowed direct observation of magnetic equator crossings in the range of distances from $\sim 2.5R_E$ (dayside) to $\sim 4.5R_E$ (nightside) during 1996 and 1997. On many passes Polar observed upper hybrid emission near the higher density regions in the vicinity of the magnetic equator as has been reported often in the past (cf. Kurth, 1982). Often this emission was accompanied by EM emission detected by the magnetic receiver of the Polar plasma wave instrument (PWI). This emission was observed simultaneously with Geotail observations of KC, when Geotail and Polar were near the same magnetic local time (MLT) and both close to the magnetic equator. Other similar EM observations were made when Polar and Geotail were well separated in MLT.

The lower resolution Polar plasma wave observations of KC are typically banded with separations in frequency consistent with the local cyclotron frequency. Spin-modulation observed by the Polar observations indicate the electric field emission is consistent with UH waves and the magnetic oscillations are consistent with Z or ordinary mode emission. However, the high resolution wideband observations of KC by Polar and Cluster show multiple, closely spaced (in frequency) bands observed by both spacecraft near the magnetic equator and within the plasmasphere indicate that the emission is not just due to $(n+1/2)$ harmonics of f_{ce}. The bands are separated in frequency much less than the local cyclotron frequency. One explanation for such an emission is that it is due to multiple sources of UH, Z, or ordinary mode emission from source regions located at different radial distances (hence frequency). A radial separation of $<1000\,\mathrm{km}$ could explain differences of f_{ce} of only a few hundred Hz. It is conceivable that density fluctuations in the form of cavities or ducts may be present (e.g., Darrouzet et al., 2002). It is also conceivable that fine structure can result from eigenmodes of upper hybrid waves trapped in a density enhancement, following a theory Yoon et al. (2000) have presented to explain auroral emissions in the same wave mode.

In this paper we show observations of Polar and Cluster wave data. High resolution waveform data from Polar is used to directly measure the polarization of continuum emission and the direction of propagation. We find that the continuum emission at high resolution has a fine structure very similar to KC emission. These data help us to better constrain the source mechanism and source region of both continuum and KC emission.

2. Instrumentation

2.1. Polar

The Polar satellite was launched in late February 1996 into a polar orbit with apogee of about $9R_E$ and a perigee of about $1.8R_E$. Polar is the first satellite to have 3 orthogonal electric antennas (Eu, Ev, and Ez), 3 triaxial magnetic search coils, and a magnetic loop antenna as well as an advanced plasma wave instrument (Gurnett et al., 1995). This combination can potentially provide the polarization and direction of the arrival of a signal without any prior assumptions.

The PWI on the Polar spacecraft is designed to provide measurements of plasma waves in the Earth's polar regions over the frequency range from 0.1 Hz to 800 kHz. Five receiver systems are used to process the data: a wideband receiver, a high-frequency waveform receiver (HFWR), a low-frequency waveform receiver, two multichannel analyzers, and a pair of sweep frequency receivers (SFR). For the high-frequency emissions of interest here, the SFR is of special interest.

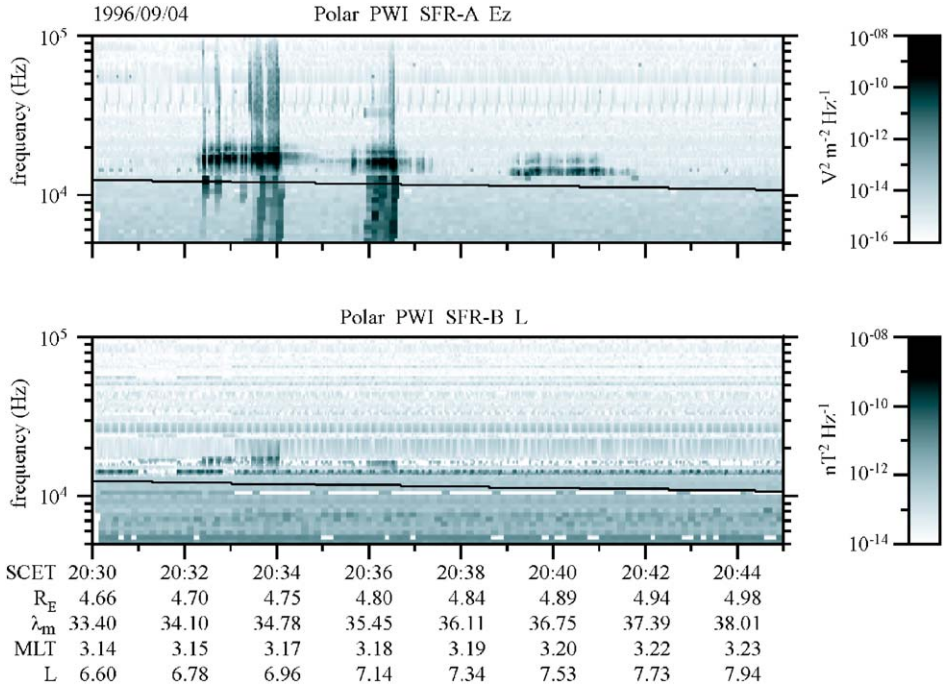

Fig. 1. A frequency-vs.-time spectrogram of the PWI sweep-frequency receiver on board Polar. We show a 15 min interval from 20:30 to 20:45 UT on September 4, 1996. The top panel is the electric field and the bottom panel is the magnetic field data. The frequency range is from 5 to 100 kHz. During this time Polar was in the pre-dawn sector at a magnetic latitude of about 34°–35° and a radial distance of about 4.75R_E. The black line indicates the local cyclotron frequency near 10 kHz.

The SFR has a frequency range from 24 Hz to 800 kHz in 5 frequency bands. The frequency resolution is about 3% at the higher frequencies. In the log mode a full frequency spectrum can be obtained every 33 s. From 12.5 to 800 kHz, of interest in this study of continuum emission, a full frequency spectrum can be obtained every 2.4 s.

The wideband receiver (WBR) provides high-resolution waveform data, and is programmable allowing the selection of 11, 22, or 90 kHz bandwidths with a lower band edge (base frequency) at 0, 125, 250, and 500 kHz. In the 90 kHz bandwidth mode the sampling rate is 249 kHz.

The HFWR measures waveform data over the frequency range of 20 Hz to 25 kHz, but also operates with a 2 kHz or 16 kHz filter. The sampling rate is 71.43 kHz in the 25 kHz mode. Typically, the receiver obtains a 0.5 s snapshot of data every 128 s.

2.2. Cluster

The Cluster II mission consists of four identical satellites in a high-inclination orbit with a nominal apogee of 12R_E and perigee of 2R_E. The mission objectives include studies of the magnetopause and magnetotail reconnection sites and magnetospheric phenomena.

The wideband plasma wave investigation on Cluster is part of the wave experiment consortium (WEC), which consists of five instruments designed specifically to study magnetospheric wave phenomena (Pedersen et al., 1997). The objective of the wideband plasma investigation is to provide very high-time resolution measurements in order to resolve spatial and temporal structure in the plasma waves and magnetosphere. The investigation consists of four identical instruments (one on each spacecraft) called the Wideband (WBD) plasma instruments. These instruments measure electric or magnetic field waveforms in one of three possible bandwidths: 25 Hz to 9.5 Hz, 50 Hz to 19 kHz, or 1–75 kHz. The base frequency (frequency offset) can be programmed to be either 125, 250, or 500 kHz. The bit rate in the real time mode of operation is 220 kbits/s.

3. Observations

In Fig. 1 we display a frequency-vs.-time spectrogram of the SFR on board Polar. We show a 15 min interval from 20:30 to 20:45 UT on September 4, 1996. The top panel is the electric field and the bottom panel is the magnetic field data. The frequency range is from 5 to 100 kHz. During this time Polar was in the pre-dawn sector at a magnetic latitude of about 34°–35° and a radial distance of about 4.75R_E. At this time the Kp was rising to about +4 at 21:00 UT and the Dst was dropping from about −3 nT at 20:00 to about −30 nT at 23:00 UT. The black line indicates the local cyclotron

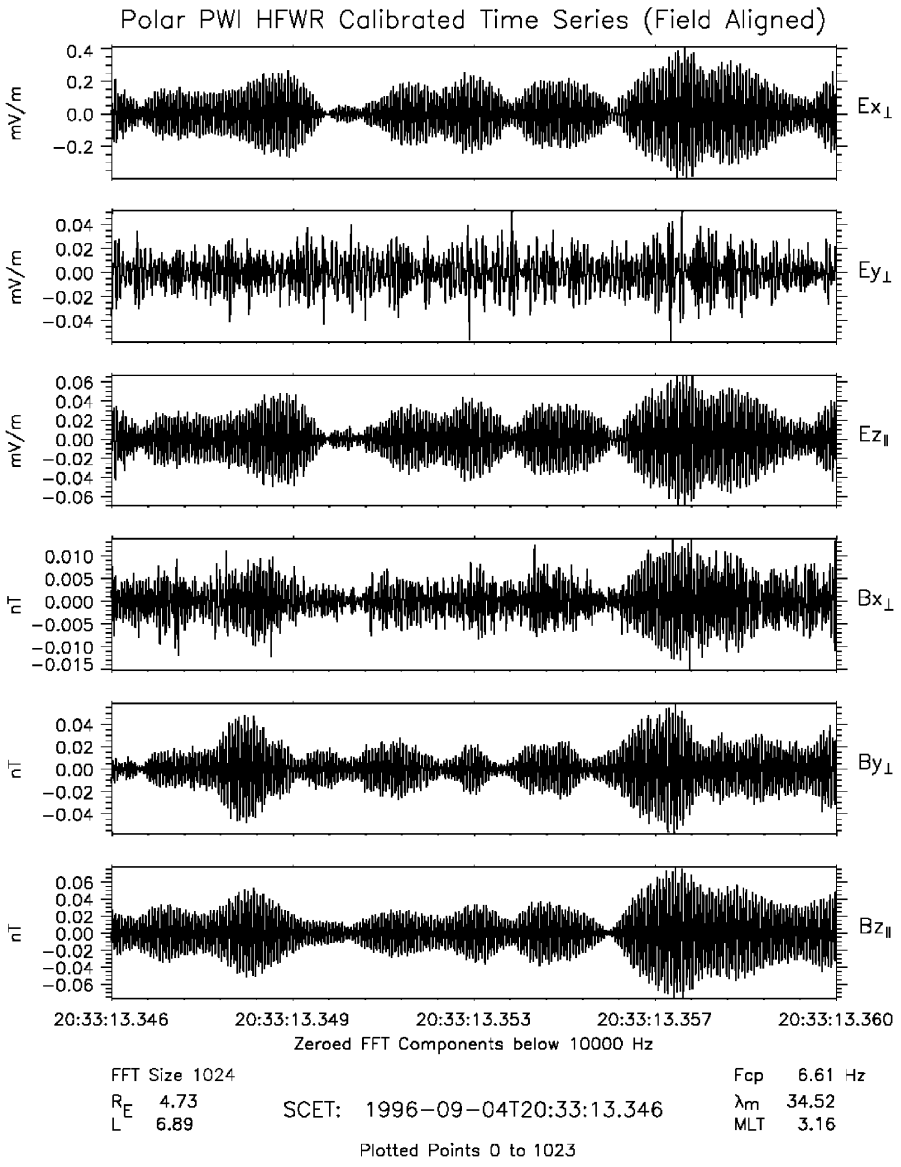

Fig. 2. A plot of the electric (top three panels) and magnetic (bottom three panels) waveforms in magnetic field-aligned coordinates. The data is a 0.014 second sub-snapshot of data starting at 20:33:13.346 of September 4, 1996. The clear electromagnetic nature of the emission is apparent. The dominant electric field is perpendicular **B**, while the perturbation magnetic field has a significant component parallel to the ambient **B**.

frequency near 10 kHz. The SFR observes intense emission that is mainly electrostatic but with some magnetic component as well. The emission is most probably upper hybrid emission with a mixture of some Z and/or O mode and we will comment on this later. This emission falls in the frequency range of continuum emission that is often observed in this region. The data looks very similar to many other passes observed by Polar and other satellites of the past such as DE-1 (cf. Morgan and Gurnett, 1991). The important thing about this data is that Polar PWI also was monitoring with the HFWR at this time.

In Fig. 2 we display a multipanel plot of the HFWR waveform data for a 14 ms snapshot of data starting at 20:33:13.346. The panels are for the electric field (top three) and magnetic field (bottom three) in field-aligned coordinates. Note the signal is electromagnetic with a predominant electric field perpendicular to B ($E_{\perp}/E_{||}\sim 5$). There is a significant component of oscillating B, however, along the ambient magnetic field. Assuming the intense electrostatic emission is upper hybrid emission we note that near 20:33:15 the most intense electric field intensities range over $14.5\,\mathrm{kHz} < f < 17.3\,\mathrm{kHz}$. The most intense emissions occur at about $f = 16\,\mathrm{kHz}$. At this time $f_{ce} = 12.2\,\mathrm{kHz}$, so using $f_{UH} = \sqrt{(f_p^2 + f_{ce}^2)}$, the range of probable values of f_p is $7.8\,\mathrm{kHz} < f_p < 12.3\,\mathrm{kHz}$. This means the range of values of the extraordinary mode cutoff, f_{RX}, is $16.0\,\mathrm{kHz} < f_{RX} < 19.8\,\mathrm{kHz}$. For $f_{UH} = 16\,\mathrm{kHz}$, $f_p = 10.35\,\mathrm{kHz}$,

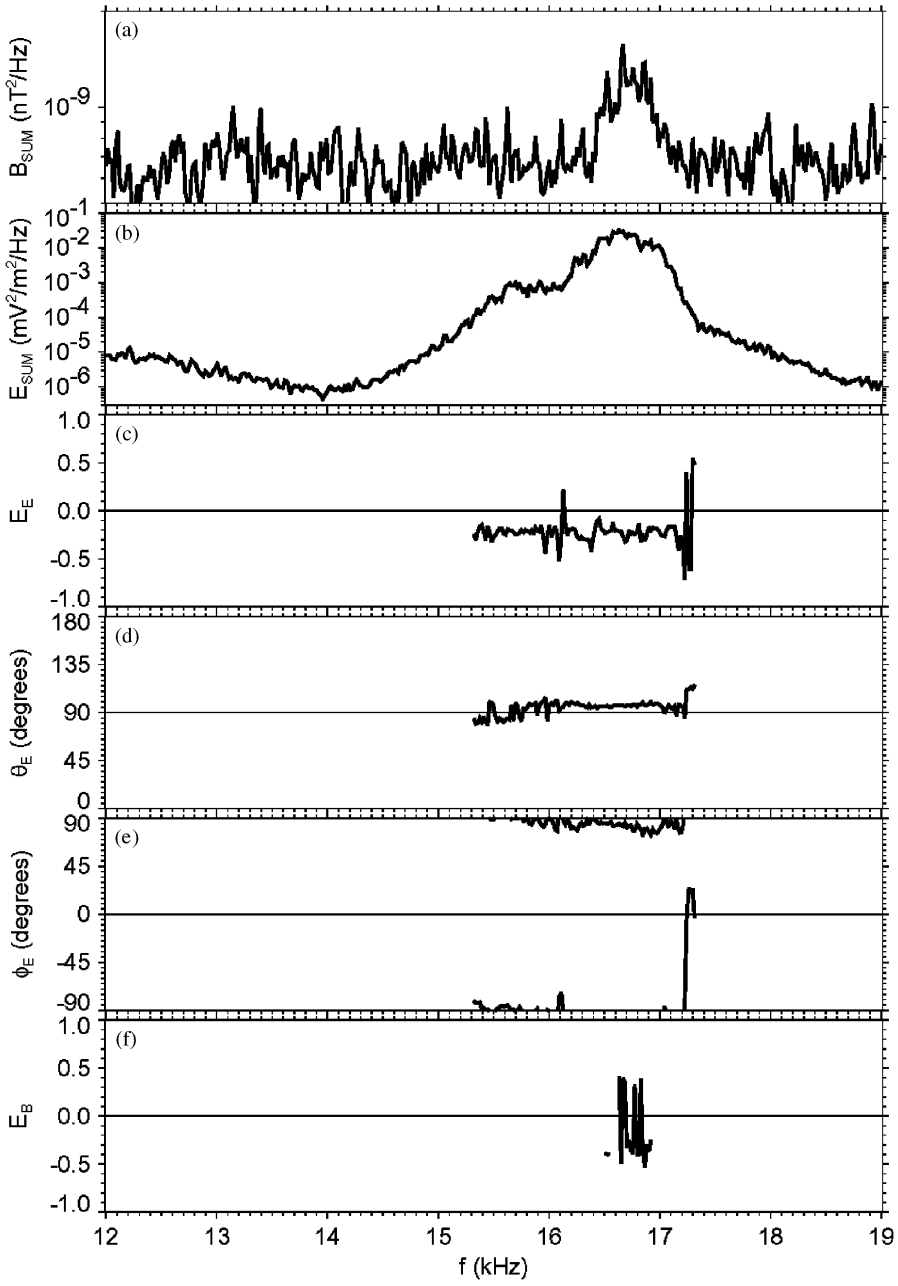

Fig. 3. Results of wave distribution function analysis for the data of Fig. 2 is shown in this multipanel plot. Seen are (from the top) magnetic power, electric field power, degree of electric polarization, polar angle (relative to **B**) of electric polarization axis (EPA), aximuthal angle of EPA, and degree of magnetic polarization.

$f_{RX} = 18.1$ kHz. From cold plasma theory we calculate, for a wave normal angle of 89°, that the index of refraction for Z mode can be large ($n > 2$) for $f \sim f_{UH}$. The most intense emission near 16 kHz is not X mode unless f_p is at the lowest probable value of 7.8 kHz. For both X and O mode the index of refraction is less than 1. Measured ratios of index of refraction evaluated by taking the ratio of cB/E are typically in the range of $10 < n < 100$. Thus, the measured and calculated index of refraction is consistent with Z mode emission.

We have also conducted wave distribution function analysis (cf. Santolik and Parrot, 2000) for a portion of this pass. Fig. 3 shows results of an analysis of the 6-component waveform measurement recorded by the HFWR instrument. The waveform capture started at 20:33:31.732, about 18 s after the waveforms of Fig. 2, and lasted for 0.445 s with a sampling frequency of 71.43 kHz. The waveforms were then subjected to a multicomponent spectral analysis using the fast Fourier transform procedure. This analysis results in a 6×6

spectral matrix at each frequency. Frequencies between 14 and 19 kHz are shown in Fig. 3.

Panels *a* and *b* represent the power-spectral densities of the magnetic and electric fields, respectively. A peak of electric power reaching $3\times10^{-2}\,mV^2\,m^{-2}\,Hz^{-1}$ is observed in this frequency range. This peak has a very weak counterpart in the magnetic field spectrum, just above the noise limit of $\sim10^{-9}\,nT^2\,Hz^{-1}$.

The polarization of the electric field fluctuations is left-handed, highly elliptical (panel *c*). The results are plotted for the electric field signal stronger than $10^{-4}\,nT^2\,Hz^{-1}$. The main polarization axis is perpendicular to the ambient magnetic field (panel *d*) oriented azimuthally in the east–west direction (panel *e*). This is indicative of the extraordinary mode. We note that the Z mode exists with left-handed extraordinary polarization for $f<f_p$, which is certainly possible at this time.

The polarization of the magnetic field fluctuations (panel *f*) is very variable and we can observe both left-handed and right-handed elliptical polarization. The interpretation of this result may be similar to that discussed by Santolik et al. (2002), where the same type of polarization was interpreted as a superposition of many linearly polarized waves. The main polarization axis deviated by less than 40° from the direction of the ambient magnetic field.

Using an analysis method based on the singular value decomposition (SVD) of the spectral matrix (Santolik et al., 2003), we find that the wave vector is close to perpendicular to the ambient magnetic field and that the waves propagate eastward, azimuthally around the Earth. The Poynting flux also probably has a northward component.

For the time of the data shown in Figs. 1 and 2 the Polar PWI wideband receiver was not selected and therefore the data were not available. In Fig. 4 we display wideband data for a pass on April 5, 1996. This is a gray-scale spectrogram for a 48-s period starting at

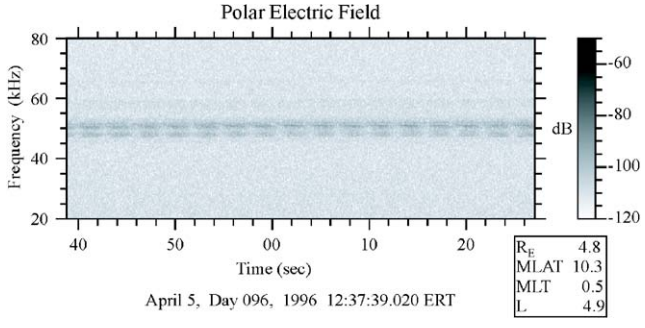

Fig. 4. Wideband spectrogram of the high resolution wideband receiver electric field data (Eu antenna) for a 48-s time interval for April 5, 1996, starting at 12:37:38.9 UT. This data covers a frequency range from 0 to about 90 kHz. Of particular significance are the many relatively intense near-constant frequency emission bands observed in the frequency range $\sim45\,kHz<f<\sim55\,kHz$. There is also a spin-modulation of the data showing nulls at ~3 s intervals.

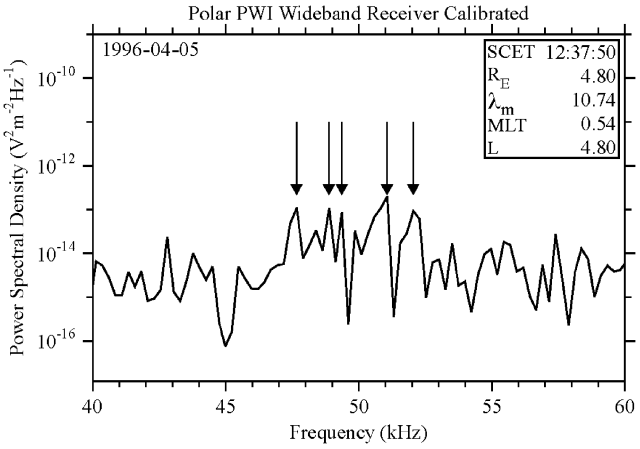

Fig. 5. A cut of the power spectral density $[V^2/(m^2\,Hz)]$ versus frequency for a small range of frequencies centered at 50 kHz. Note the series of closely spaced peaks (indicated with arrows) with separations of about 1–2 kHz. These peaks correspond to the band of emission seen in Fig. 4.

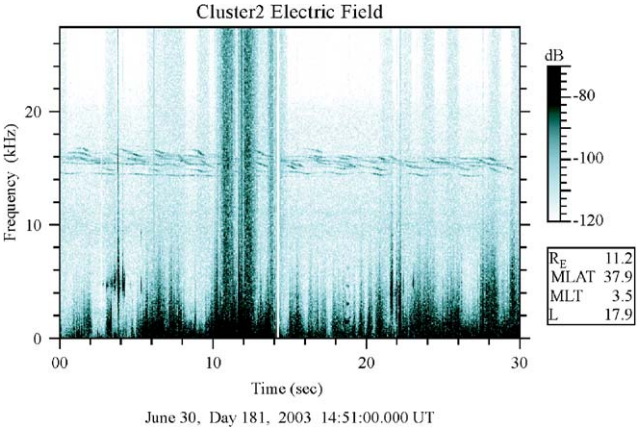

Fig. 6. A spectrogram of the wideband instrument (WBD) on board the Cluster (C2) spacecraft. The spectrogram covers a frequency range from 0 to 28 kHz over a 30-s time interval for the electric field (Ez antenna). C2 is located at a magnetic latitude of $\lambda_m = 37.9$, $R = 11.2R_E$ and MLT ~3.5 h. Seen in the figure in the frequency range $14\,kHz<f<17\,kHz$ are very many closely spaced emission bands that appear to oscillate in frequency with an amplitude of a few hundred Hz.

12:37:38.9, when the spacecraft was located near a magnetic local time of midnight, magnetic latitude of 13 degrees, and radial distance of about $4.9R_E$. At this time the Kp is 1 and the Dst is about −8 nT decreasing only slowly. The local cyclotron frequency was about 7.1 kHz. We observe several bands of continuum emission, with each band separated by a frequency much less than f_{ce}. There is a definite spin modulation of the signal with nulls occurring every 3 s (the spacecraft spin period is about 6 s). We have determined that the electric field nulls occur when the electric field antennas in the spin plane are nearly parallel with **B** and the

intensity peaks are centered when the same antennas are nearly orthogonal to **B**. This would be consistent with Z-mode or X-mode. In order to clearly display the closely spaced bands of emission, we plot in Fig. 5 a cut of the power spectral density [$V^2/(m^2\,Hz)$] versus frequency for a small range of frequencies centered at 50 kHz. A series of peaks with separations of about 1–2 kHz is seen. We have used a 1024 point FFT and the sampling rate of the data is 249 kHz, so the frequency resolution is about 365 Hz. This figure is very similar to Figs. 9 and 10 of Menietti et al. (2003) which show KC emission observed also by the wideband receiver. The biggest difference would be the frequency range. The data of Fig. 4 require a similar explanation as that provided for the KC. We suggest that there are multiple closely spaced sources of emission possibly associated with density structures.

Finally, in Fig. 6 we show an example of Cluster data obtained when the C2 spacecraft was located at MLT = 3.5, magnetic latitude of 37.9°, and a radial distance of $11.2R_E$. This large radial distance means that the spacecraft is well outside the plasmasphere and not near a source of continuum emission. The Kp is about 3.5 and the Dst is relatively steady at −21 nT. The spectrogram format is similar to Fig. 4, but the time duration of the plot is 30 s. Seen in this figure are low-frequency electrostatic emissions and what appears to be continuum emission in the frequency range $14\,kHz < f < 17\,kHz$. The plasma frequency is not known, but due to the spacecraft position we can be certain that $f_p << 14\,kHz$, thus the emission is in a free-space mode. The emission shows an unusual fine structure with separations much less than f_{ce}, which is about 2.8 kHz at this time. The fine structures appear to have an oscillating frequency with an ampltitude of about a few hundred Hz. The source of these oscillations is only speculative, but may be due to a perturbation of the source region.

4. Summary and conclusions

The wideband observations of Polar and Cluster continuum emission provide new and interesting information. Multiple closely spaced (in frequency) bands observed by both the spacecraft near and outside the plasmasphere indicate that the emission is not just due to $(n+1/2)$ harmonics of f_{ce}. One explanation for such an emission is that it is due to multiple sources of UH or Z mode emission from source regions located at different radial distances (hence frequency). This explanation would be consistent with source regions associated with distinct density structures as have been reported in the past for the plasmapause (cf. LeDocq et al., 1994; Darrouzet et al., 2002; Menietti et al., 2003). Such structures may take the form of ducts (enhancements) or cavities.

The source mechanism of continuum emission has been generally described by the linear conversion theory of Jones (1988) and by the nonlinear conversion mechanisms described by Melrose (1981), Barbosa (1982), or Ronnmark (1983, 1989, 1992). All of these mechanisms involve upper hybrid waves. In the linear mechanism UH waves refract (in a steep density gradient) to Z-mode waves at a wave normal angle near 90°. Z-mode waves can mode convert to O-mode waves (cf. Horne, 1989, 1990). The nonlinear mechanisms are described by the authors as more efficient than the linear conversion mechanism. The polarization obtained by Polar for the data of Figs. 1 and 2 would indicate that the most predominant polarization is Z-mode. This does not preclude that O or even X mode is not present at lower intensity.

Eigenmode trapping of Z-mode emissions for both density cavities and density enhancements (cf. McAdams et al., 2000; Yoon et al., 2000) has been suggested to explain discrete emissions (fine structure) of auroral roar. A modification of such processes might also explain the present observations.

The observations of continuum emission are in every way analogous to the observations of KC emission presented by Menietti et al. (2003). This is strong evidence that both continuum and KC have similar source mechanisms, and most probably are associated with density structures in the plasmasphere and plasmapause region. A comprehensive study of these density structures using the Cluster spacecraft will be most important.

Acknowledgments

The authors thank J. Hospodarsky for text editing, and A. Persoon for assistance with graphical editing. The research at Iowa was supported by NASA grant NAG5-11942 and by NSF award No. 0307319/ME650.

References

Barbosa, D.D., 1982. Low-level VLF and LF radio emissions observed at Earth and Jupiter. Rev. Geophys. 20, 316–334.

Brown, L.W., 1973. The galactic radio spectrum between 130 and 2600 kHz. Astrophys. J. 180, 359–370.

Budden, K.G., 1980. The theory of radio windows in the ionosphere and magnetosphere. J. Atmos. Terr. Phys. 180, 287–298.

Darrouzet, F., Lemaire, J., Decreau, P.M.E., Trotignan, J.G., Rauch, J.L., Le Guirriec, E., Randriamboarison, O., Canu, P., Moullard, O., Masson, A., Sedgemore, F., 2002. Multipoint observation of small scale irregularities at the plasmapause, using the Whisper measurements. Paper presented at the International Union of Radio Science, The Netherlands.

Fung, S.F., Papadopoulos, K., 1987. The emission of narrow-band Jovian kilometric radiation. J. Geophys. Res. 92, 8579–8593.

Green, J.L., Sandel, B.R., Fung, S.F., Gallagher, D.L., Reinisch, B.W., 2002. On the origin of kilometric continuum. J. Geophys. Res. 107 (A7), 1105.

Gurnett, D.A., 1974. The Earth as a radio source: terrestrial kilometric radiation. J. Geophys. Res. 79, 4227–4238.

Gurnett, D.A., 1975. The earth as a radio source: the nonthermal continuum. J. Geophys. Res. 80, 2751–2763.

Gurnett, D.A., Shaw, R.R., 1973. Electromagnetic radiation trapped in the magnetosphere above the plasma frequency. J. Geophys. Res. 78, 8136–8149.

Gurnett, D.A., Persoon, A.M., Randall, R.F., Odem, D.L., Remington, S.L., Averkamp, T.F., DeBower, M.M., Hospodarsky, G.B., Huff, R.L., Kirchner, D.L., Mitchell, M.A., Pham, B.T., Phillips, J.R., Schintler, W.J., Sheyko, P., Tomash, D.R., 1995. The Polar plasma wave instrument. Space Sci. Rev. 71, 597–622.

Hashimoto, K., Calvert, W., Matsumoto, H., 1999. Kilometric continuum detected by Geotail. J. Geophys. Res. 104, 28645–28656.

Horne, R.B., 1989. Path-integrated growth of electrostatic waves: the generation of terrestrial myriametric radiation. J. Geophys. Res. 94, 8895–8909.

Horne, R.B., 1990. Narrow-band structure and amplitude of terrestrial myriametric radiation. J. Geophys. Res. 95, 3925–3932.

Jones, D., 1976. Source of terrestrial non-thermal continuum radiation. Nature 260, 686–689.

Jones, D., 1988. Planetary radio emissions from low magnetic latitudes: observations and theories. In: Rucker, H.O., Bauer, S.J., Pedersen, B.-M. (Eds.), Planetary Radio Emissions II. Austrian Academy of Sciences, Graz, pp. 255–293.

Kasaba, Y., Matsumoto, H., Hashimoto, K., Anderson, R.R., Bougeret, J.-L., Kaiser, M.L., Wu, X.Y., Nagano, I., 1998. Remote sensing of the plasmapause during substorms: Geotail observation of nonthermal continuum enhancement. J. Geophys. Res. 103 (A9), 20389–20405.

Kurth, W.S., 1982. Detailed observations of the source of terrestrial narrowband electromagnetic radiation. Geophys. Res. Lett. 9, 1341–1344.

Kurth, W.S., 1992. Continuum radiation in planetary magnetospheres. In: Rucker, H.O., Bauer, S.J., Kaiser, M.L. (Eds.), Planetary Radio Emissions III. Austrian Academy of Science, pp. 329–350.

Kurth, W.S., Gurnett, D.A., Anderson, R.R., 1981. Escaping non-thermal continuum radiation. J. Geophys. Res. 86, 5519–5531.

LeDocq, M.J., Gurnett, D.A., Anderson, R.R., 1994. Electron number density fluctuations near the plasmapause observed by CRRES spacecraft. J. Geophys. Res. 99, 23661–23671.

McAdams, K.L., Ergun, R.E., LaBelle, J., 2000. HF chirps: eigenmode trapping in density depletions. J. Geophys. Res. 27, 321–324.

Melrose, D.B., 1981. A theory for the nonthermal radio continua in the terrestrial and Jovian magnetospheres. J. Geophys. Res. 86, 30–36.

Menietti, J.D., Anderson, R.R., Pickett, J.S., Gurnett, D.A., Matsumoto, H., 2003. Near-source and remote observations of kilometric continuum radiation from multi-spacecraft observations. J. Geophys. Res. 108 (A11), 1393.

Morgan, D.D., Gurnett, D.A., 1991. The source location and beaming of terrestrial continuum radiation. J. Geophys. Res. 86, 9595–9613.

Pedersen, A., Cornilleau-Wehrlin, N., de la Porte, B., Roux, A., Bouabdellah, A., Decreau, P.M.E., Lefeuvre, F., Sene, F.X., Gurnett, D., Huff, R., Gustafsson, G., Holmgren, G., Woolliscroft, L., Alleyne, H.S., Thompson, J.A., Davies, P.H.N., 1997. The wave experiment consortium (WEC). Space Sci. Rev. 79, 93–105.

Ronnmark, K., 1983. Emission of myriametric radiation by coalescence of upper hybrid waves with low frequency waves. Ann. Geophys. 1, 187–192.

Ronnmark, K., 1989. Myriametric radiation and the efficiency of linear mode conversion. Geophys. Res. Lett. 16, 731–738.

Ronnmark, K., 1992. Conversion of upper hybrid waves into magnetospheric radiation. In: Rucker, H.O., Bauer, S.J., Kaiser, M.L. (Eds.), Planetary Radio Emissions III. Austrian Academy of Science, pp. 405–417.

Santolik, O., Parrot, M., 2000. Application of wave distribution function methods to an ELF hiss event at high latitudes. J. Geophys. Res. 105, 18885–18894.

Santolik, O., Pickett, J.S., Gurnett, D.A., Storey, L.R.O., 2002. Magnetic component of narrow-band ion cyclotron waves in the auroral zone, J. Geophys. Res. 107 (A12), 1444.

Santolik, O., Parrot, M., Lefeuvre, F., 2003. Singular value decomposition methods for wave propagation analysis. Radio. Sci. 38 (1), 1010.

Yoon, P.H., Weatherwax, A.T., LaBelle, J., 2000. Discrete electrostatic eigenmodes associated with ionospheric density structure: generation of auroral roar fine frequency structure. J. Geophys. Res. 105, 27589–27596.